ACS APPLIED MATERIALS & INTERFACES

www.acsami.org

Research Article

Multimode Visualization of Electronic Skin from Bioinspired Colorimetric Sensor

Jingxuan Xu,[†] Chaoyi Ban,[†] Fei Xiu,* Zhihui Tian, Wenjie Jiang, Minjie Zhang, Heshan Zhang, Zhe Zhou, Juqing Liu,* and Wei Huang*

Cite This: *ACS Appl. Mater. Interfaces* 2021, 13, 30205−30212

Read Online

ACCESS | Metrics & More | Article Recommendations | Supporting Information

ABSTRACT: Bioskins possess a great ability to detect and deliver external mechanical or temperature stimuli into identifiable signals such as color changes. However, the integration of visualization with simultaneous detection of multiple complex external stimuli in a single biosensor device remains a challenge. Here we propose an all-solution-processed bioinspired stretchable electronic skin with interactive color changes and four-mode sensing properties. The fabricated biosensor demonstrates sensitive responses to various stimuli including pressure, strain, voltage, and temperature. Sensing visualization is realized by color changes of the e-skin from brown to green and finally bright yellow as a response to intensified external stimuli, suggesting great application potential in military defense, healthcare monitoring, and smart bionic skin.

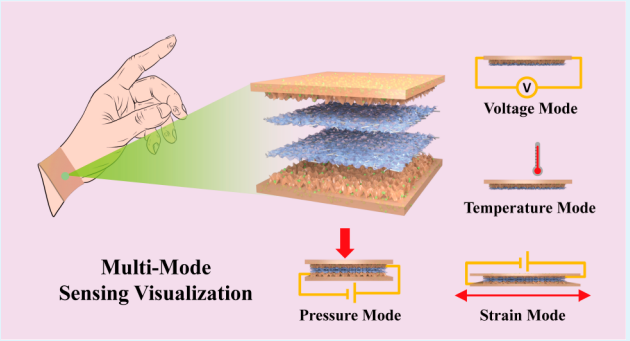

KEYWORDS: *multimode, colorimetric, sensor, visualization, electronic skin*

INTRODUCTION

Skin reveals extensively attractive features including flexibility, stretchability, tactile sensing, color changes, and so on. Skin-inspired electronics or electronic skin (e-skin) are referred and pursued by utilizing electronic devices to mimic or even transcend such excellent properties of biological skin.[1,2] Skin-inspired electronics can precisely detect and monitor external mechanical or electrical stimuli directly from the surface of the skin.[3,4] Collected stimuli are commonly delivered into identifiable or quantitative electrical signals, showing attractive applications in robotics,[5−7] human−machine interfaces (HMIs),[8,9] and human health monitoring systems.[10−13] Ideal electronic skins are expected to possess satisfactory flexibility and stretchability and multimode sensing as well as a visible response to external physical signals.[14] Moreover, better biological compatibility of artificial e-skin materials with human skin or smart robots is also desired and of great significance in addition to pursuing the performance.[1,14]

Investigations of skinlike tactile sensing functionality through the material and structural design of electronics have been widely demonstrated recently.[15,16] Notably, early skin-inspired electronics development is focused on improving the performance of single-mode flexible sensors. The developed electronic skins can well mimic diversified sensing behaviors of biological skins based on a single response mode for pressure sensing,[15,17,18] strain sensing,[19,20] temperature sensing,[21,22] and so on. Particularly, Bao and colleagues successfully demonstrated a chameleon-inspired stretchable e-skin for pressure visualization, in which the applied pressure on the e-skin can be directly expressed through color changes, endowing visualization function of the e-skin sensor.[23] With the increasing demands of multifunctional electronic skin, significant advances have been made in the development of two- or three-mode bionic sensors recently via structural design or material exploration.[24−26] For instance, Park et al. reported a dual-mode e-skin with pressure and temperature dual-mode sensing functions by integrating capacitive sensor and piezoresistive sensor together into a single taxel.[24] A skin-inspired multisensory e-skin integrating specific extensible sensor units was proposed that was capable of simultaneously sensing of temperature, in-plane strain, humidity, light, magnetic field, pressure, and proximity.[25] Particularly, sensing visualization via color-change control makes huge contributions to the development of bioinspired sensor devices, which has been realized through steam stimulation, temperature stimulation, acidity/alkalinity, or chemical reaction, combing adaptive deformation functions.[27−29] Despite these achievements, the sensitive and simultaneous detection of multiple complex external stimuli with a single device remains a

Received: April 21, 2021
Accepted: June 3, 2021
Published: June 17, 2021

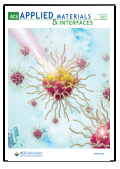

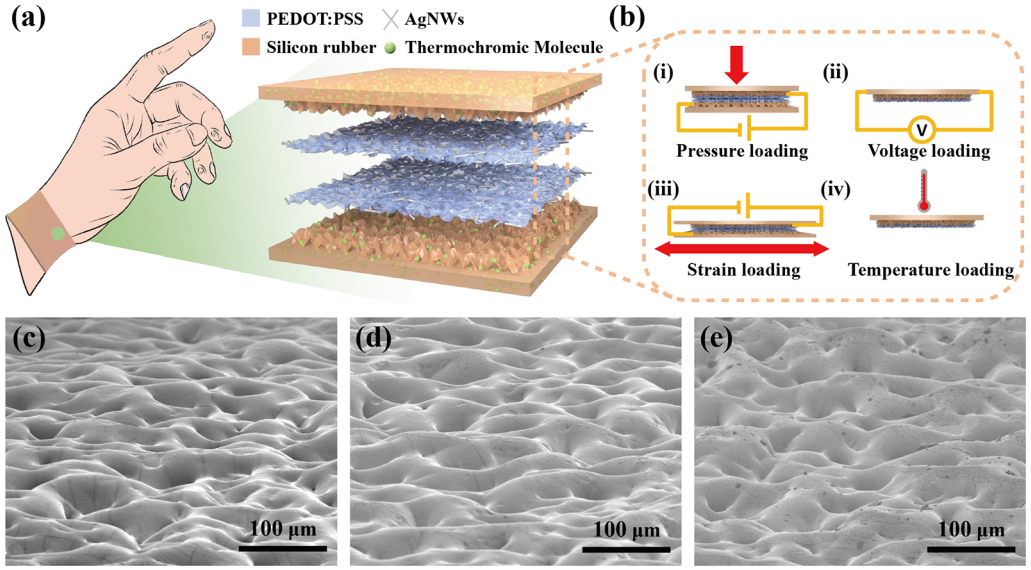

Figure 1. Inspiration, mechanism, and structure of stretchable multimode colorimetric sensor based on bioskin. (a) Structure and material selection of bioinspired colorimetric sensors. (b) Schematics of bioinspired multimode colorimetric sensor under pressure load (a-i), voltage load (a-ii), tension load (a-iii), and heating stimulation (a-iv). (c) Scanning electronic microscopy (SEM) of a molded of silicon rubber film with the similar microstructure to that of abrasive paper no. 320. (d) SEM observation of colorimetric silicon rubber substrate mixed with thermochromic molecules. (e) SEM observation of colorimetric silicon rubber thin film after AgNW deposition and PEDOT:PSS coating.

challenge. Moreover, there is still an urgent need to explore a biocompatible and more sensing-mode electronic skin that responds to diversified stimuli.

In this work, we report a bionic electronic skin holding four-mode sensing ability, sensing visualization based on a simple sensor device with hierarchical face-to-face asymmetric microstructures. The fabricated stretchable electronic skin demonstrates interactive color changes from brown to green and finally bright yellow, responding to intensified external stimuli including pressure, strain, voltage, and temperature, showing excellent performance in applications of interactive wearable devices, health monitoring, military application, and smart robotics. The artificial reconstruction of four sensing modes corresponds to different combination manners of three electrodes in one device and their working mechanisms are discussed in detail. Moreover, commercial silicon rubber, which is a promising biomaterial for artificial organs, is used as the e-skin substrate, and it shows excellent biological compatibility.

RESULTS AND DISCUSSION

Humans possess the capability to change their skin color when they suffer from certain external mechanical force, such as a press or a pinch; the surrounding skin will appear white and reddish because of the lack or accumulation of blood. Moreover, shy people blush because of subcutaneous telangiectasia congestion. Similarly, when the human body is close to a heat source (for example, hot water), the nervous system immediately regulates blood flow in order to dissipate heat, which also causes the skin turn to red. Bioinspired by the natural sensing response and the epidermis tissue structure of human skin, we proposed a multimode colorimetric bionic sensor device with a hierarchical face-to-face asymmetric microstructure consisting of a PEDOT:PSS protecting layer, a AgNW electron transfer layer, and a silicon rubber substrate mixed with thermochromic molecules (Figure 1a). The fabricated skin-inspired sensor can detect diversified stimuli (including pressure, tension, voltage, and temperature), and these four artificially reconstructed sensing modes correspond to different combinations of the device electrodes. As shown in Figure 1b, there are three electrodes in the sensor. When different electrodes are used under external stimuli, the device turns out different sensing mechanisms. When connecting the upper and lower electrodes, and giving a certain initial constant voltage, the conduction path is very small because of limited contact area between the upper and lower irregular microstructures, and almost no Joule heat is generated. When an external pressure load is applied (Figure 1b(i)), the conduction pathways in the device increase because of squeezing between the upper and lower microstructures under external pressure, leading to more Joule heat generation as well as temperature improvement. For the voltage-sensing mode, when applying a voltage on the monolayer of the e-skin by connecting the two electrodes on the same side, the current in the circuit gives rise to the generation of Joule heat (Figure 1b(ii)). Similarly, when a tensile load is applied, the contact area between the top and bottom electrodes increases dramatically under tensile deformation, corresponding to the generation of Joule heat (Figure 1b(iii)). Specifically, abundant thermochromic molecules incorporated in the silicon rubber substrate turn out different colors as a visual response to the increasing Joule heat generated under enhancing stimuli.[30−32] When no voltage is applied, the monolayer of the e-skin film can also change colors as the external temperatures increases, suggesting temperature-sensing function (Figure 1b(iv)). Therefore, multimode electronic skin holds the merit that it can present colorimetric discoloration when responding to different magnitudes of applied stimuli to realize sensing visualization. We have analyzed multifunctional visual unit sensors published in recent years, and device performances are summarized in the Table S1. It should be noted that most of these published works were focused on the exploration of bionic sensor device with only one or dual functions. Few research studies refer to sensing visualization and the sensitive detection of multiple

https://doi.org/10.1021/acsami.1c07360
ACS Appl. Mater. Interfaces 2021, 13, 30205−30212

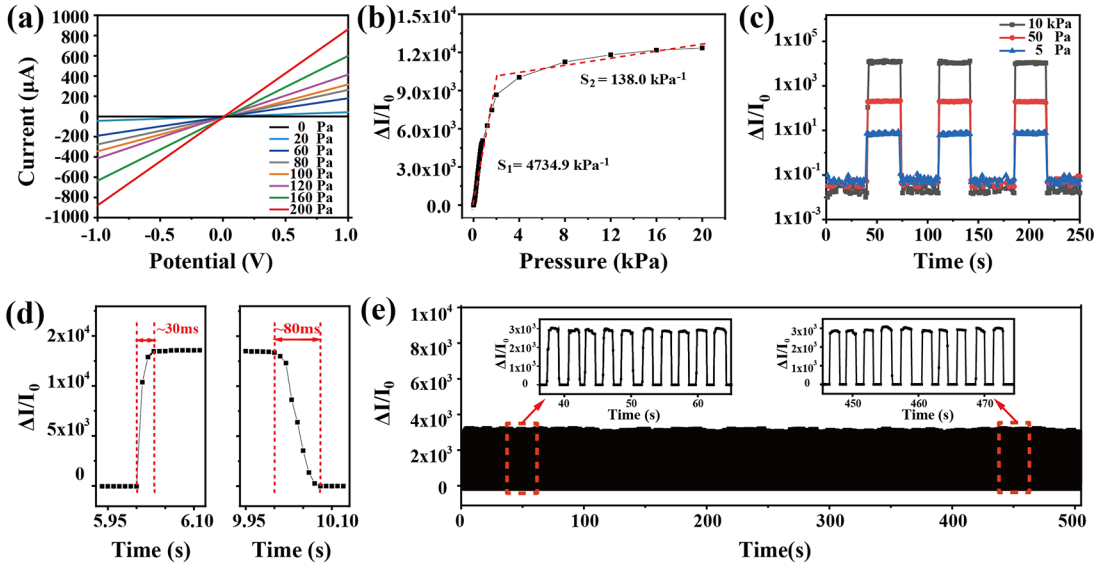

Figure 2. Electromechanical properties of the randomly distributed spinosum pressure sensor. (a) The $I-V$ curves of the pressure sensor using abrasive paper no. 320, the linear dependence of voltage on current under different pressures verifies the ohmic contacts between AgNws and the electrodes. (b) Sensitivities of pressure sensor during the pressure from 0 to 20 kPa. (c) Relative current changes of the pressure sensor subjected to loading/unloading cycles at various applied pressures. (d) Real-time fast response and release of the pressure sensor upon 20 kPa pressure. (e) Excellent cycle stability performance of the device after a 500 s pressure cycling test under 500 Pa.

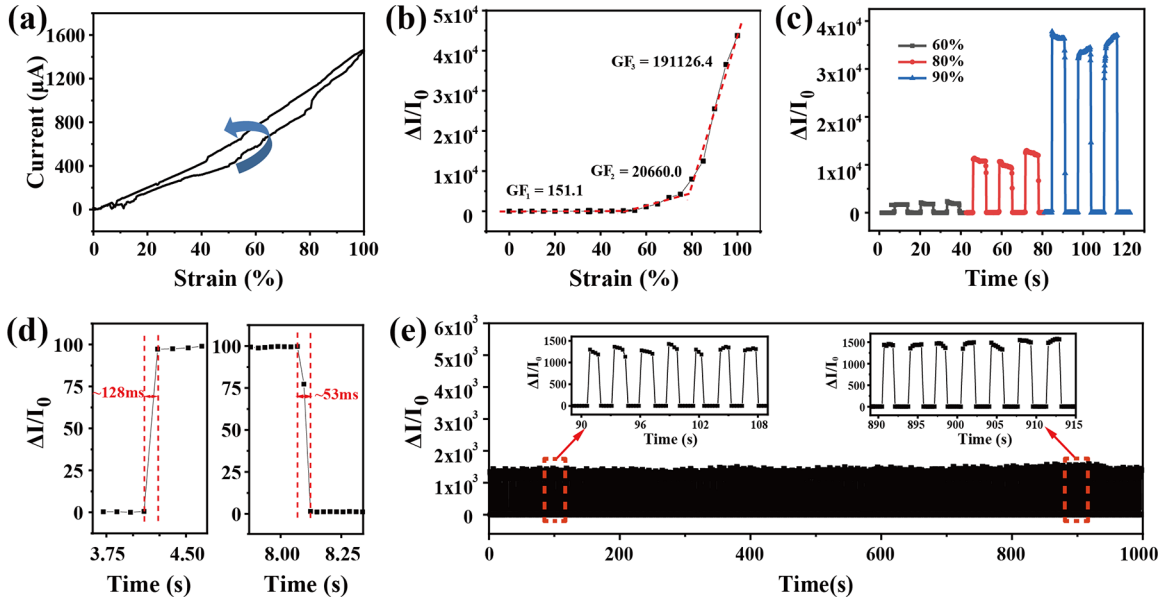

Figure 3. Electromechanical properties of the randomly distributed spinosum strain sensor. (a) Hysteresis curves for the randomly distributed strain sensor. (b) Typical relative resistance-strain curve of the strain sensor within 100% strain. (c) Reliability test of the strain sensor under repeated cycles of stretching and releasing at different applied stretches. (d) Real-time fast response and release of the strain sensor with the strain of 5%. (e) Excellent cycle stability performance of the device after a 1000 s tension cycling test within 60% strain.

complex external stimuli within a single device. Even though Zhang et al. designed a sensor device that integrated the four modes of pressure, stretching, temperature, and humidity, its visualization function could not be realized on a macroscopic level.[33]

Bioinspired by the abrasive paperlike topography of the human epidermis surface, we use an abrasive paper (2 × 2 cm^2) as the template to prepare a micropatterned thermochromic molecule/silicon rubber thin film with a random height distribution through a coating−pilling procedure. The scanning electronic microscopy (SEM) image of the micropatterned silicon rubber substrate using no. 320 abrasive paper is shown in Figure 1c. The morphology of the spinosum silicon rubber shows smoothly interconnected ridges and dispersive pores, demonstrating similar micropatterns to that of the abrasive paper. Because of the small size (microcapsules 1−10 μm in diameter) of the thermochromic molecular materials,[34,35] mixing in the silicone rubber substrate did not affect the surface spinous process morphology (Figure 1d). After depositing a thin layer of conducting AgNW to effectively transport electrons, a protective PEDOT:PSS layer is drop-coated subsequently to prevent AgNWs being destroyed and guarantee a good adhesion of AgNWs to silicon rubber, which plays a significant role in deciding the lifetime of sensors.[36−38]

https://doi.org/10.1021/acsami.1c07360
ACS Appl. Mater. Interfaces 2021, 13, 30205−30212

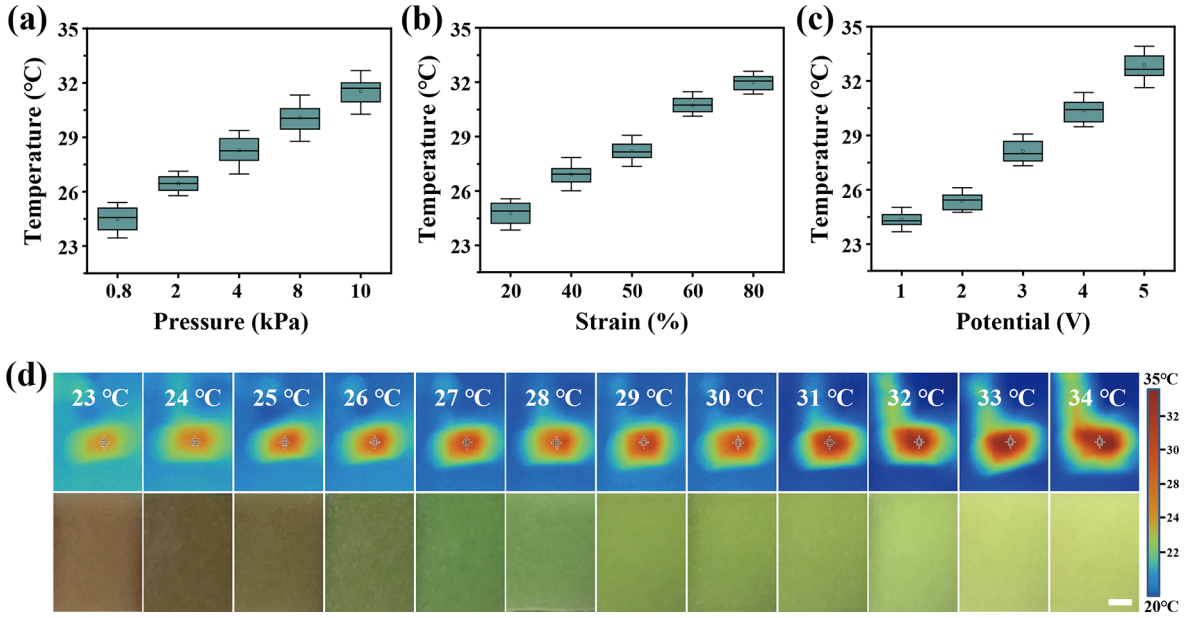

Figure 4. Multimode visualization of colorimetric sensors and its thermal characteristic. (a) Heating behavior of the colorimetric sensor under different pressures. (b) Heating behavior of the colorimetric sensor under different stretches. (c) Heating behavior of the colorimetric sensor under various working voltages. (d) Digital image of the colorimetric sensor at different temperatures using a thermal imaging analysis instrument. (All pictures are captured at the same magnified pixels with a scale bar of 0.25 cm.)

The SEM (Figure 1e) and cross-section SEM characterization (Figure S1a, b) of the PEDOT:PSS/AgNW/silicon rubber sample exhibit the well-maintained morphology of the silicon rubber with low roughness, demonstrating that a uniform PEDOT:PSS thin film as well as a AgNW layer has covered the silicon rubber surface. The average length and diameter of the AgNWs are about 10 μm (Figure S1c, d) and 33 nm (Figure S1e, f), respectively. Finally, a face-to-face packaging is applied to fabricate the integrated multimode colorimetric sensor.

Figure 2a presents current−potential (I−V) curves of the fabricated biosensor under different applied pressures, where the linear I−V relationship indicates the ohmic contact characteristic. The slope of the I−V curves increases with increasing pressure, revealing a stable response of the biosensor to static pressure. Figure 2b shows the relative resistance variation versus pressure, from which two linear resistance segments including a sharp decrease in the low-pressure range and a gradual decrease in the high-pressure range are clearly observed. The sensitivity of a sensor, which is expressed as $(R_0 - R)/(R_0P)$, is usually used to evaluate performance of a pressure sensor, where R_0 and R are the initial resistance and resistance under applied pressure, respectively. For the sensor prepared using abrasive paper no. 320, its sensitivity is calculated to be 4734.9 and 138.0 kPa^{-1} in a pressure range of 0−2 kPa and a higher-pressure range, respectively. Figure 2c exhibits the electrical response of the biosensor to repeated loading/unloading cycles at various applied pressures. The current changes sharply and repeatedly during loading/unloading cycles, indicating an excellent accuracy and reliability of the sensor. Moreover, Figure 2d demonstrates a remarkably short response time with a rise time of 30 ms and drop time of 80 ms, which is beneficial to detecting various vigorous human motion signals such as breathing rate, pulse, and running speed. Hysteresis of the response time is mainly attributed to the elastic recovery of the silicon rubber substrate. To further evaluate the durability and reliability of our sensor, we performed multiple loading/unloading cycles by applying a pressure of 500 Pa, as shown in Figure 2e. Figure 2e shows that the relative current change is almost constant during 500 s load/unloading cycles and magnified electrical responses (Figure 2e inset) are almost identical and sharp in each cycle, indicating excellent sensing durability and stability. Compared with abrasive paper-templated pressure sensors currently published (Table S2), our pressure sensor demonstrates excellent sensitivity, a fast response time, and a low detection limit.

Figure 3a shows the hysteresis curve with loading and unloading of randomly distributed spinosum strain sensor, from which the hysteresis data of electrical resistance under applied strain is observed to be negligible, indicating a good reversible property of the sensor. Moreover, resistance variation ratios ($\Delta R/R_0 = (R_\varepsilon - R_0)/R_0$; R_0 and R_ε corresponds to the resistance without and with tensile, respectively) monitored by stretching strains are investigated to test the performance of this strain sensor. The sensitivity of the device is indicated by the gauge factor (GF), which is defined as GF = $\delta(\Delta R/R_0)/\delta_\varepsilon$; ε is the stretch strain of the device ($\varepsilon = (L - L_0)/L_0$, where L_0 and L are the lengths of the sensor before and after stretching). Figure 3b demonstrates relative electricity changes of the strain sensor under increasing strain. As the applied strain ε increases from 0 to 50%, the relative electricity changes ($\Delta R/R_0$) slowly and linearly with the GF calculated to be 151.1. When applied strain >50%, GF of the strain sensor is calculated to be 20 660.0 (ε = 50−75%), and 191126.4 (ε = 75−100%), suggesting an excellent linear sensing behavior. Figure 3c shows that the compressive strain sensor possesses ultrastable and distinguishable response with excellent repeatability to different compressive strains of 60, 80, and 90%. Furthermore, the response time of the stretchable multimode colorimetric strain sensors is investigated. Figure 3d shows that when 50% strain is loaded, a response time of 128 ms and release time of 53 ms is realized. To investigate the cyclic durability and reproducibility of the sensor, we have the strain sensor perform a release−compression cycle for 1000 s

https://doi.org/10.1021/acsami.1c07360
ACS Appl. Mater. Interfaces 2021, 13, 30205−30212

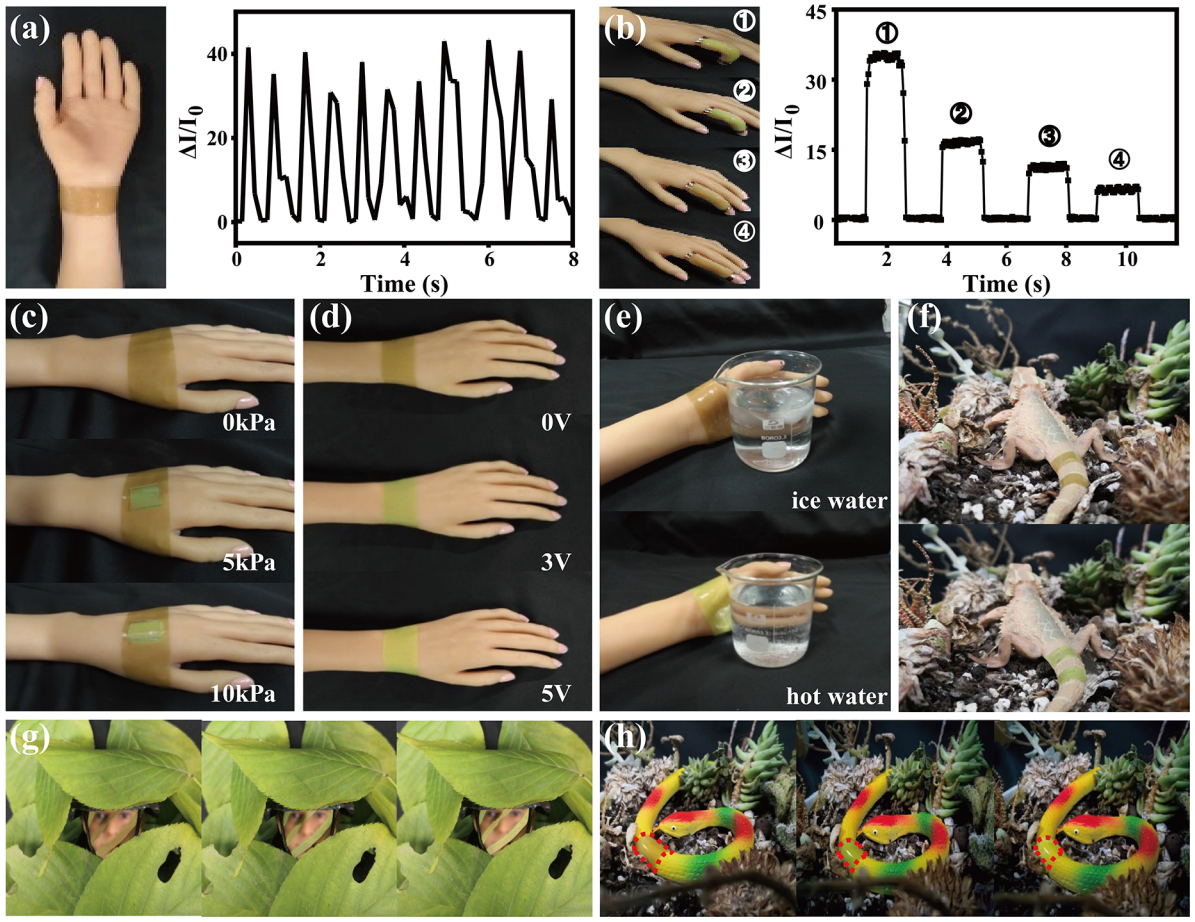

Figure 5. Demonstration of practical application scenario photographs of a multimode colorimetric sensor in the different modes. (a) Photograph of the colorimetric sensor attached at the wrist as a pulse sensor and the record of the pulse wave. (b) Photograph and amplified waveform of the colorimetric sensor attached to the index finger. Digital images of the colorimetric sensor under (c) various applied pressures, (d) different working voltages, and (e) different working temperature. (f–h) Digital images of the potential application value of the colorimetric sensor.

under a compressive of strain 60%, as shown in Figure 3e. Obviously, $\Delta I/I_0$ of the strain sensor could maintain favorable repeatability, suggesting excellent response stability.

Electric heating behaviors of the multimode sensor responding to applied voltage as well as mechanical forces are investigated. Figure 4a–c shows that the temperature of the central region of the sensor measured via a thermal imaging analysis instrument increases rapidly with increasing applied pressure, tension, and working voltage. During these three stimulation modes, the current of the sensor device increases as applied stimulus intensifies, leading to dramatically increased generation of Joule heating and improved temperature of the sensor device. Moreover, it is obvious from the Joule heating formula that the temperature of the e-skin will increase gradually with prolonged time of stimulation.[35] We have supplemented the temperature–time dependence test of the colorimetric sensor under pressure (Figure S2a), strain (Figure S2b), and voltage (Figure S2c) control to support the Figure 4a–c. Furthermore, to reveal the visualization feature of our colorimetric sensor, relationship between bioskin color and device temperature is investigated using a digital camera to record the color change process of the bioskin from 23 to 34 °C (Figure 4d) under a certain external stimulus at room temperature (20 °C). In addition, the multimode colorimetric electronic skin can not only intuitively map stimuli through color changes but also quantitatively feedback external stimuli through the current, as shown in Figure S3. This dual-response mechanism provides users with visible interaction and anti-interference capabilities, endowing this electronic skin more application potentials. As shown in Figure S4, when the pressure sensor is under no load and 10 kPa pressure, the contact resistance is almost unchanged under different temperature conditions. It should be observed that the bioskin initially exhibits brown color when no stimulus is applied. When loading a stimulus, the color of the bioskin presents a gradual change from brown to green and finally to bright yellow as the bioskin temperature increases. The presented distinct color difference of the bioskin could be explained by the color response of the thermochromic molecules mixed in the silicon rubber to the surrounding temperature change that is caused by electric heating induced by resistance variation. This colorimetric visualization feature of the multimode sensor is beneficial to accurately detect and monitor the external stimuli, enabling the prepared bioskin to have diversified practical applications.

Combining great merits of stretchability, biocompatibility, accurate visualization, and excellent multimode sensing properties, the fabricated electronic skin possesses enormous application potential. By wearing such a biosensor on the wrist, real-time pulse signals under relaxation conditions could be detected and recorded as real-time electrical current change (Figure 5b), from which repeatable and regular pulse signals

https://doi.org/10.1021/acsami.1c07360
ACS Appl. Mater. Interfaces 2021, 13, 30205–30212

with 75 beats min^{-1} frequency are observed, close to the normal level of humans, suggesting excellent accuracy of this biosensor. Moreover, the colorimetric biosensor can be fixed on fingers to visually detect finger movements basing on the strain mode of the sensor. Figure 5b shows that as bending angle of the target finger increases, the sensor demonstrates interactive color changes from brown green to bright yellow because of the improved device temperature caused by decreased resistance. The above initial investigations indicate a great application potential of this colorimetric multimode biosensor in healthcare monitoring and smart robotics applications. The visualization characteristic of our colorimetric sensor responding to pressure, voltage, and temperature is further investigated in Figure 5c–e. Obviously, when a 5 kPa load (one piece of glass slice) is loaded on the back of hand, the sensor device turns bright green from the initial brown color (Figure 5c). When the pressure load increases to 10 kPa (two pieces of glass slice), the color of the device changes to yellow. In addition, an interactive color change from brown to green to yellow is observed as an increasing voltage is applied (Figure 5d). The device also exhibits apparent response to the external temperature, which shows bright yellow when close to a heat source (hot water) and turns brown when close to ice water (Figure 5e), endowing this biosensor potential applications in wearable devices for temperature monitoring. Benefiting from this excellent colorimetric visualization feature, our fabricated colorimetric biosensor is expected to inspire further research in developing military applications or intelligent skin (Figure 5f–h). Such an outstanding stimulus–response property of the biosensor allows the electronic skin to mimic or even transcend natural human skin.

CONCLUSIONS

In summary, we have successfully demonstrated a bioinspired stretchable electronic skin capable of interactive color changes and four-mode sensing properties. Sensing visualization of the e-skin is realized by color changes from brown to green and finally bright yellow as a response to intensified external stimuli including pressure, tension, voltage, and temperature. The artificial reconstruction of these four sensing modes is demonstrated to correspond to different combination manners of three electrodes in one device. Moreover, the all-solution-processing approach and material used in the biosensor fabrication suggests a low-power-consumption sensing system with excellent biological compatibility. Combining the above merits, the biosensor exhibits good reversible properties and excellent repeatability and stability, enabling the prepared e-skin to mimic or even transcend natural human skin and endowing it with potential applications in interactive wearable devices, health monitoring, military application, and smart robotics.

EXPERIMENTAL SECTION

Pretreatment of Abrasive Paper Materials. Commercial abrasive papers with a roughness of 320, were selected as templates. To remove impurities, abrasive papers were washed with deionized water and ethanol solvent, respectively. Surfaces were then blown dry with a nitrogen gun to get pieces of precleaned microstructural templates.

Preparation of Patterned and Colorimetric Substrate. The thermochromic silicon prepolymer was prepared by mixing base silicone rubber and curing agent well with thermochromic materials (TM), in a weight ratio of 10:1:0.5. The mixture was poured into a Petri dish with a precleaned abrasive paper template. The Petri dish was then slammed down several times to remove air bubbles created during the mixing process and placed in natural conditions for 6 h to form a thin film, which was carefully peeled off the abrasive paper to get a micropatterned silicone rubber thin film. Before coating the electrode material, the film was pretreated with UV ozone for 20 min.

Preparation of Top and Bottom Electrode. Silver nanowires with a sheet resistance of ~20 Ω sq^{-1} were sprayed on the pretreated film at 50 °C, by using an air gun. The synthesis of the AgNWs can be seen in our previous report. The AgNW film is treated with oxygen plasma at 30 w for 10 s. The PEDOT:PSS aqueous phase dispersion was premixed with 5% DMSO and stirred well, which has been proven to improve the conductivity of PEDOT:PSS by up to 2–3 orders of magnitude. The premixed PEDOT:PSS solution was then dripped onto the oxygen-treated AgNW film, following which the excess PEDOT:PSS mixed solution was obliquely flowed out. After a thermal curing process at 80 °C for 15 min on a heating platform, a wrinkled conductive film was obtained.

Fabrication of Multimode Sensor. First, the copper wire was fixed to the wrinkled conductive film with a silver paste. Note that each paste in one film should not touch the conductive part of the other film. Two qualified conducting films were then assembled face to face with patterned surfaces touching each other.

Characterization. The microstructures of the patterned films were characterized by a field-emission SEM (JSM-7800F). The current–time (I–T) measurements were tested by a Keithley 4200 semiconductor parameter analyzer under ambient conditions. The response to the applied pressure was performed by gently loading different weights of objects onto the pressure sensor, corresponding to different pressures. Similarly, the response to the applied strain was performed by gently stretching the pressure sensor to different lengths, corresponding to the different strain. The area was calculated on the basis of the contact surface. The temperature measurements were performed with an thermal imaging analysis instrument. Physical images were taken with a digital camera. All electrical measurements were carried out in an ambient air environment.

ASSOCIATED CONTENT

Supporting Information

The Supporting Information is available free of charge at https://pubs.acs.org/doi/10.1021/acsami.1c07360.

Cross-section and enlarged SEM of PEDOT:PSS-AgNW-silicon film; characterization and analysis of the aspect ratio of AgNW; time-dependent temperature in different modes; electrical signals under different modes; current changes at different temperatures; summary of multifunctional visual unit sensor performances; summary of abrasive paper-templated pressure sensor performances (Figures S1–S4, Tables S1 and S2) (PDF)

AUTHOR INFORMATION

Corresponding Authors

Fei Xiu – *Key Laboratory of Flexible Electronics (KLOFE) & Institute of Advanced Materials (IAM), Nanjing Tech University (NanjingTech), Nanjing 211816, China*; Email: iamfxiu@njtech.edu.cn

Juqing Liu – *Key Laboratory of Flexible Electronics (KLOFE) & Institute of Advanced Materials (IAM), Nanjing Tech University (NanjingTech), Nanjing 211816, China*; orcid.org/0000-0002-6499-2796; Email: iamjqliu@njtech.edu.cn

Wei Huang – *Key Laboratory of Flexible Electronics (KLOFE) & Institute of Advanced Materials (IAM), Nanjing Tech University (NanjingTech), Nanjing 211816, China; Shaanxi Institute of Flexible Electronics (SIFE), Northwestern Polytechnical University (NPU), Xi'an*

https://doi.org/10.1021/acsami.1c07360
ACS Appl. Mater. Interfaces 2021, 13, 30205–30212

710072, China; Key Laboratory for Organic Electronics and Information Displays & Institute of Advanced Materials (IAM), Nanjing University of Posts & Telecommunications (NUPT), Nanjing 210023, China; orcid.org/0000-0001-7004-6408; Email: wei-huang@njtech.edu.cn

Authors

Jingxuan Xu − *Key Laboratory of Flexible Electronics (KLOFE) & Institute of Advanced Materials (IAM), Nanjing Tech University (NanjingTech), Nanjing 211816, China*

Chaoyi Ban − *Key Laboratory of Flexible Electronics (KLOFE) & Institute of Advanced Materials (IAM), Nanjing Tech University (NanjingTech), Nanjing 211816, China*

Zhihui Tian − *Key Laboratory of Flexible Electronics (KLOFE) & Institute of Advanced Materials (IAM), Nanjing Tech University (NanjingTech), Nanjing 211816, China*

Wenjie Jiang − *Key Laboratory of Flexible Electronics (KLOFE) & Institute of Advanced Materials (IAM), Nanjing Tech University (NanjingTech), Nanjing 211816, China*

Minjie Zhang − *Key Laboratory of Flexible Electronics (KLOFE) & Institute of Advanced Materials (IAM), Nanjing Tech University (NanjingTech), Nanjing 211816, China*

Heshan Zhang − *Key Laboratory of Flexible Electronics (KLOFE) & Institute of Advanced Materials (IAM), Nanjing Tech University (NanjingTech), Nanjing 211816, China*

Zhe Zhou − *Key Laboratory of Flexible Electronics (KLOFE) & Institute of Advanced Materials (IAM), Nanjing Tech University (NanjingTech), Nanjing 211816, China*

Complete contact information is available at: https://pubs.acs.org/10.1021/acsami.1c07360

Author Contributions

†J.-X.X. and C.-Y.B. contributed equally to this work. F.X., J.-Q.L., and W.H. conceived and supervised the experiments. J.-Q.L., W.H., J.-X.X., and C.-Y.B. proposed ideas and formulated overarching research goals. J.-X.X. and C.-Y.B. performed the fabrication and electrical measurements of electronic skin. Z.-H.T. and M.-J.Z. assisted with the synthesis of materials. W.-J.Z., H.-S.Z., and Z.Z. assisted the characterization of samples. J.-X.X., C.-Y.B., and F.X. prepared the initial draft. All authors discussed the results and commented on the manuscript.

Notes

The authors declare no competing financial interest.

■ ACKNOWLEDGMENTS

We acknowledge the primary financial support by the National Key R&D Program of China (2017YFB1002900), the National Natural Science Foundation of China (61622402, 51703093), the Natural Science Foundation of Jiangsu (BK20171000), and the Jiangsu Specially-Appointed Professor programme, the Six Talent Plan (2015XCL015).

■ REFERENCES

(1) Yang, J. C.; Mun, J.; Kwon, S. Y.; Park, S.; Bao, Z.; Park, S. Electronic Skin: Recent Progress and Future Prospects for Skin-Attachable Devices for Health Monitoring, Robotics, and Prosthetics. *Adv. Mater.* **2019**, *31*, 1904765.

(2) Wang, M.; Luo, Y.; Wang, T.; Wan, C.; Pan, L.; Pan, S.; He, K.; Neo, A.; Chen, X. Artificial Skin Perception. *Adv. Mater.* **2021**, *33*, 2003014.

(3) Wang, S.; Oh, J. Y.; Xu, J.; Tran, H.; Bao, Z. Skin-Inspired Electronics: An Emerging Paradigm. *Acc. Chem. Res.* **2018**, *51*, 1033−1045.

(4) Chortos, A.; Bao, Z. Skin-Inspired Electronic Devices. *Mater. Today* **2014**, *17*, 321−331.

(5) Zhang, C.; Liu, S.; Huang, X.; Guo, W.; Li, Y.; Wu, H. A Stretchable Dual-Mode Sensor Array for Multifunctional Robotic Electronic Skin. *Nano Energy* **2019**, *62*, 164−170.

(6) Liu, S.; Wang, S.; Xuan, S.; Zhang, S.; Fan, X.; Jiang, H.; Song, P.; Gong, X. Highly Flexible Multilayered E-Skins for Thermal-Magnetic-Mechanical Triple Sensors and Intelligent Grippers. *ACS Appl. Mater. Interfaces* **2020**, *12*, 15675−15685.

(7) Chen, H.; Song, Y.; Guo, H.; Miao, L.; Chen, X.; Su, Z.; Zhang, H. Hybrid Porous Micro Structured Finger Skin Inspired Self-Powered Electronic Skin System for Pressure Sensing and Sliding Detection. *Nano Energy* **2018**, *51*, 496−503.

(8) Won, P.; Park, J. J.; Lee, T.; Ha, I.; Han, S.; Choi, M.; Lee, J.; Hong, S.; Cho, K. J.; Ko, S. H. Stretchable and Transparent Kirigami Conductor of Nanowire Percolation Network for Electronic Skin Applications. *Nano Lett.* **2019**, *19*, 6087−6096.

(9) Guo, Y.; Guo, Z.; Zhong, M.; Wan, P.; Zhang, W.; Zhang, L. A Flexible Wearable Pressure Sensor with Bioinspired Microcrack and Interlocking for Full-Range Human-Machine Interfacing. *Small* **2018**, *14*, 1803018.

(10) Wang, Y.; Chao, M.; Wan, P.; Zhang, L. A Wearable Breathable Pressure Sensor from Metal-Organic Framework Derived Nanocomposites for Highly Sensitive Broad-Range Healthcare Monitoring. *Nano Energy* **2020**, *70*, 104560.

(11) Ge, G.; Cai, Y.; Dong, Q.; Zhang, Y.; Shao, J.; Huang, W.; Dong, X. A Flexible Pressure Sensor Based on RGO/Polyaniline Wrapped Sponge with Tunable Sensitivity for Human Motion Detection. *Nanoscale* **2018**, *10*, 10033−10040.

(12) Yin, F.; Li, X.; Peng, H.; Li, F.; Yang, K.; Yuan, W. A Highly Sensitive, Multifunctional, and Wearable Mechanical Sensor Based on RGO/Synergetic Fiber Bundles for Monitoring Human Actions and Physiological Signals. *Sens. Actuators, B* **2019**, *285*, 179−185.

(13) Wang, S.; Gong, L.; Shang, Z.; Ding, L.; Yin, G.; Jiang, W.; Gong, X.; Xuan, S. Novel Safeguarding Tactile E-Skins for Monitoring Human Motion Based on SST/PDMS-AgNW-PET Hybrid Structures. *Adv. Funct. Mater.* **2018**, *28*, 1707538.

(14) Lee, Y.; Park, J.; Choe, A.; Cho, S.; Kim, J.; Ko, H. Mimicking Human and Biological Skins for Multifunctional Skin Electronics. *Adv. Funct. Mater.* **2020**, *30*, 1904523.

(15) Pang, Y.; Zhang, K.; Yang, Z.; Jiang, S.; Ju, Z.; Li, Y.; Wang, X.; Wang, D.; Jian, M.; Zhang, Y.; Liang, R.; Tian, H.; Yang, Y.; Ren, T. L. Epidermis Microstructure Inspired Graphene Pressure Sensor with Random Distributed Spinosum for High Sensitivity and Large Linearity. *ACS Nano* **2018**, *12*, 2346−2354.

(16) Yang, C.; Li, L.; Zhao, J.; Wang, J.; Xie, J.; Cao, Y.; Xue, M.; Lu, C. Highly Sensitive Wearable Pressure Sensors Based on Three-Scale Nested Wrinkling Microstructures of Polypyrrole Films. *ACS Appl. Mater. Interfaces* **2018**, *10*, 25811−25818.

(17) Niu, H.; Gao, S.; Yue, W.; Li, Y.; Zhou, W.; Liu, H. Highly Morphology-Controllable and Highly Sensitive Capacitive Tactile Sensor Based on Epidermis-Dermis-Inspired Interlocked Asymmetric-Nanocone Arrays for Detection of Tiny Pressure. *Small* **2020**, *16*, 1904774.

(18) Cheng, Y.; Ma, Y.; Li, L.; Zhu, M.; Yue, Y.; Liu, W.; Wang, L.; Jia, S.; Li, C.; Qi, T.; Wang, J.; Gao, Y. Bioinspired Microspines for a High-Performance Spray Ti3C2Tx MXene-Based Piezoresistive Sensor. *ACS Nano* **2020**, *14*, 2145−2155.

(19) Zhao, Y.; Huang, Y.; Hu, W.; Guo, X.; Wang, Y.; Liu, P.; Liu, C.; Zhang, Y. Highly Sensitive Flexible Strain Sensor Based on Threadlike Spandex Substrate Coating with Conductive Nanocomposites for Wearable Electronic Skin. *Smart Mater. Struct.* **2019**, *28*, 035004.

(20) Guo, X.; Huang, Y.; Zhao, Y.; Mao, L.; Gao, L.; Pan, W.; Zhang, Y.; Liu, P. Highly Stretchable Strain Sensor Based on SWCNTs/CB Synergistic Conductive Network for Wearable Human-Activity Monitoring and Recognition. *Smart Mater. Struct.* **2017**, *26*, 095017.
(21) Yang, H.; Qi, D.; Liu, Z.; Chandran, B. K.; Wang, T.; Yu, J.; Chen, X. Soft Thermal Sensor with Mechanical Adaptability. *Adv. Mater.* **2016**, *28*, 9175−9181.
(22) Wang, F.; Jiang, J.; Sun, F.; Sun, L.; Wang, T.; Liu, Y.; Li, M. Flexible Wearable Graphene/Alginate Composite Non-Woven Fabric Temperature Sensor with High Sensitivity and Anti-Interference. *Cellulose* **2020**, *27*, 2369−2380.
(23) Chou, H.-H.; Nguyen, A.; Chortos, A.; To, J. W.; Lu, C.; Mei, J.; Kurosawa, T.; Bae, W.-G.; Tok, J. B.-H.; Bao, Z. A Chameleon-Inspired Stretchable Electronic Skin with Interactive Colour Changing Controlled by Tactile Sensing. *Nat. Commun.* **2015**, *6*, 8011.
(24) Kim, J.-O.; Kwon, S. Y.; Kim, Y.; Choi, H. B.; Yang, J. C.; Oh, J.; Lee, H. S.; Sim, J. Y.; Ryu, S.; Park, S. Highly Ordered 3D Microstructure-Based Electronic Skin Capable of Differentiating Pressure, Temperature, and Proximity. *ACS Appl. Mater. Interfaces* **2019**, *11*, 1503−1511.
(25) Hua, Q.; Sun, J.; Liu, H.; Bao, R.; Yu, R.; Zhai, J.; Pan, C.; Wang, Z. L. Skin-Inspired Highly Stretchable and Conformable Matrix Networks for Multifunctional Sensing. *Nat. Commun.* **2018**, *9*, 244.
(26) Zhang, Z.; Chen, Z.; Wang, Y.; Zhao, Y. Bioinspired Conductive Cellulose Liquid-Crystal Hydrogels as Multifunctional Electrical Skins. *Proc. Natl. Acad. Sci. U. S. A.* **2020**, *117*, 18310−18316.
(27) Wang, Y.; Cui, H.; Zhao, Q.; Du, X. Chameleon-Inspired Structural-Color Actuators. *Matter* **2019**, *1*, 626−638.
(28) Du, X.; Cui, H.; Xu, T.; Huang, C.; Wang, Y.; Zhao, Q.; Xu, Y.; Wu, X. Reconfiguration, Camouflage, and Color-Shifting for Bioinspired Adaptive Hydrogel-Based Millirobots. *Adv. Funct. Mater.* **2020**, *30*, 1909202.
(29) Wei, S.; Lu, W.; Le, X.; Ma, C.; Lin, H.; Wu, B.; Zhang, J.; Theato, P.; Chen, T. Bioinspired Synergistic Fluorescence-Color-Switchable Polymeric Hydrogel Actuators. *Angew. Chem., Int. Ed.* **2019**, *58*, 16243−16251.
(30) Park, B.; Kim, J. U.; Kim, J.; Tahk, D.; Jeong, C.; Ok, J.; Shin, J. H.; Kang, D.; Kim, T.-I. Strain-Visualization with Ultrasensitive Nanoscale Crack-Based Sensor Assembled with Hierarchical Thermochromic Membrane. *Adv. Funct. Mater.* **2019**, *29*, 1903360.
(31) Lee, G.; Bae, G. Y.; Son, J. H.; Lee, S.; Kim, S. W.; Kim, D.; Lee, S. G.; Cho, K. User-Interactive Thermotherapeutic Electronic Skin Based on Stretchable Thermochromic Strain Sensor. *Adv. Sci.* **2020**, *7*, 2001184.
(32) Xu, M.; Li, F.; Zhang, Z.; Shen, T.; Zhang, Q.; Qi, J. Stretchable and Multifunctional Strain Sensors Based on 3D Graphene Foams for Active and Adaptive Tactile Imaging. *Sci. China Mater.* **2019**, *62*, 555−565.
(33) Zhang, S.; Wu, R.; Lv, J. Smart Thermometer Style Sensor with Volume Readout and Visualization for pH Detection. *Arabian J. Chem.* **2020**, *13*, 8524−8531.
(34) Lim, J.-E.; Lee, S.-M.; Kim, S.-S.; Kim, T.-W.; Koo, H.-W.; Kim, H.-K. Brush-Paintable and Highly Stretchable Ag Nanowire and PEDOT:PSS Hybrid Electrodes. *Sci. Rep.* **2017**, *7*, 14685.
(35) Lee, J.; Kim, G.; Shin, D.-K.; Park, J. Solution-Processed Resistive Pressure Sensors Based on Sandwich Structures Using Silver Nanowires and Conductive Polymer. *IEEE Sens. J.* **2018**, *18*, 9919−9924.
(36) Chen, S.; Li, S.; Peng, S.; Huang, Y.; Zhao, J.; Tang, W.; Guo, X. Silver Nanowire/Polymer Composite Soft Conductive Film Fabricated by Large-Area Compatible Coating for Flexible Pressure Sensor Array. *J. Semicond.* **2018**, *39*, 013001.
(37) Yang, M.; Pan, J.; Luo, L.; Xu, A.; Huang, J.; Xia, Z.; Cheng, D.; Cai, G.; Wang, X. CNT/Cotton Composite Yarn for Electro-Thermochromic Textiles. *Smart Mater. Struct.* **2019**, *28*, 085003.
(38) Ge, F.; Fei, L.; Zhang, J.; Wang, C. The Electrical-Triggered High Contrast and Reversible Color-Changing Janus Fabric Based on Double Side Coating. *ACS Appl. Mater. Interfaces* **2020**, *12*, 21854−21862.

https://doi.org/10.1021/acsami.1c07360
ACS Appl. Mater. Interfaces 2021, 13, 30205−30212